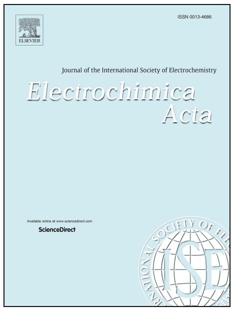

Realising the activity benefits of Pt preferential (111) surfaces for ethanol oxidation in a nanowire electrocatalyst

Edmundo S.V. Neto, Caio V.S. Almeida, Andrea E. Russell, Giancarlo R. Salazar-Banda, Katlin I.B. Eguiluz

PII: S0013-4686(20)30598-3
DOI: https://doi.org/10.1016/j.electacta.2020.136206
Reference: EA 136206

To appear in: *Electrochimica Acta*

Received Date: 13 December 2019
Revised Date: 17 March 2020
Accepted Date: 6 April 2020

Please cite this article as: E.S.V. Neto, C.V.S. Almeida, A.E. Russell, G.R. Salazar-Banda, K.I.B. Eguiluz, Realising the activity benefits of Pt preferential (111) surfaces for ethanol oxidation in a nanowire electrocatalyst, *Electrochimica Acta* (2020), doi: https://doi.org/10.1016/j.electacta.2020.136206.

CRediT author statement

Edmundo S. V. Neto: Acquisition, analysis and interpretation of the data, Methodology, Investigation, Writing - Original Draft.

Caio V. S. Almeida: Acquisition, analysis and interpretation of the data, Methodology, Investigation, Writing - Original Draft.

Andrea E. Russell: Formal analysis, Writing - Review & Editing, Visualization.

Giancarlo R. Salazar-Banda: Project administration, Supervision, Funding acquisition, conceptualization and planning of the work and Writing - Review & Editing.

Katlin I. B. Eguiluz: Project administration, Supervision, Funding acquisition, conceptualization and planning of the work and Writing - Review & Editing.

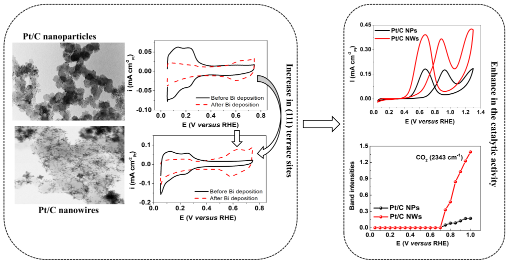
Pt/C nanoparticles
Pt/C nanowires
i (mA cm$^{-2}_{Pt}$)
0.05
0.00
-0.05
-0.10
0.0
0.2
0.4
0.6
0.8
E (V *versus* RHE)
Before Bi deposition
After Bi deposition
0.1
0.0
-0.1
-0.2
Increase in (111) terrace sites
Enhance in the catalytic activity
Pt/C NPs
Pt/C NWs
I (mA cm$^{-2}_{Pt}$)
0.45
0.30
0.15
0.00
1.0
1.2
1.4
Band intensities
CO$_2$ (2343 cm^{-1})
1.5
1.2
0.9
0.6
0.3
0.0

Realising the activity benefits of Pt preferential (111) surfaces for ethanol oxidation in a nanowire electrocatalyst

Edmundo S. V. Neto,[a,b] Caio V. S. Almeida, [a,b] Andrea E. Russell,[c] Giancarlo R. Salazar-Banda,[a,b] Katlin I. B. Eguiluz*[a,b]

[a] Laboratory of Electrochemistry and Nanotechnology, Institute of Technology and Research, 49.032-490, Aracaju, Sergipe, Brazil.

[b] Processes Engineering Post-Graduate Program, Tiradentes University, 49.032-490, Aracaju, Sergipe, Brazil.

[c] School of Chemistry, University of Southampton, University Road, Southampton SO17 1BJ, United Kingdom.

* Corresponding Author: katlinbarrios@gmail.com

Abstract

The commercialisation of direct ethanol fuel cells (DEFCs) is hindered by the low activity of the currently available electrocatalysts that are mainly carbon-supported nanoparticles (NPs). Here, we synthesised carbon-supported Pt nanowires (Pt/C NWs) by chemical reduction of metallic precursors at room temperature without using surfactants, templates, or stabilising agents. The synthesised Pt NWs were supported on high surface area carbon (Vulcan XC-72R) with 40 wt%. of metal loading concerning the support. The electroactivity of the synthesised NWs catalyst towards ethanol and CO (the dominant intermediate species) oxidation is investigated and tested in comparison with a commercial nanoparticle Pt/C electrocatalyst (named: Pt/C NPs). The electrooxidation of ethanol was investigated in acid media by CO-stripping, cyclic voltammetry, derivative voltammetry, chronoamperometry, steady-state polarisation curves, and *in situ* Fourier transform infrared spectroscopy (FTIR) experiments. The results showed that the synthesised Pt NWs are much more active than the Pt/C NPs catalyst, for both ethanol and CO-monolayer oxidation in acidic media. *In situ* FTIR data revealed that Pt NWs catalyst favours the formation of CO_2 and acetic acid. This activity is mainly due to the existence of extended terraces, resulting in enhanced mobility of OH_{ads} and CO_{ads}, facilitating the removal of CO_{ads} from the catalyst surface and allowing better ethanol adsorption for further oxidation. Hence, 5-fold higher current density for ethanol oxidation is obtained. The NW morphology of Pt nanocatalysts results in very active materials towards ethanol oxidation and may provide a promising means of increasing the performance of anodes for DEFCs.

Keywords: Nanowires; Ethanol electro-oxidation; Current density; Adsorption.

1. Introduction

Increasing environmental protection concerns and the increasing world energy consumption have resulted in a major quest for the development of cleaner and alternative energy production systems, preferentially those not working with fossil fuels. In this context, small-scale generation systems, such as wind turbines, solar energy, and fuel cells (FCs), play an essential role in meeting global needs through distributed generation [1]. FCs are very attractive devices able to obtain directly the electric energy contained in fuels (commonly H_2 or liquid fuels like methanol and ethanol), releasing water as a principal by-product [1,2].

In FCs, the direct conversion nature avoids mechanical frictional losses, increasing the fuel overall conversion efficiency. Moreover, these systems are not limited by the thermodynamic constraints derived from the Carnot cycle [3]. Most of the studies have been focused on using hydrogen as fuel; however, difficulties in transportation, stocking, and distribution hinder the FCs further application. Thus, by using liquid fuels, such as methanol or ethanol, the need to adapt or re-establish the existing infrastructure (as required for hydrogen) can be reduced. As methanol is a toxic fuel, ethanol appears as a viable alternative [4].

Ethanol is a C-2 containing alcohol with important features, such as non-toxicity, large scale production from biomass, easy transportation and storage, high energy density (8.0 kWh kg^{-1}), and high solubility in aqueous electrolytes [2,5] that make it attractive for sustainable energy applications. In addition, ethanol possesses approximately two-thirds of the energy density of pure gasoline [6,7]. In the USA and Brazil, ethanol has a well-established distribution network, being available in many gas/petrol stations, unlike methanol [8].

The energy delivered from a direct ethanol fuel cell (DEFC) is theoretically higher than at a direct methanol fuel cell (DMFC, 8.0 kWh kg^{-1} *versus* 6.1 kWh kg^{-1}, respectively), thus reducing the fuel consumption [6]. However, the complete ethanol oxidation reaction (EOR) is still a challenge due to the complexity of the reaction. The total oxidation of ethanol involves the cleavage of the C–C bond and the transfer of 12 electrons (e^{-}) per ethanol molecule [9]. There is a consensus that the partial ethanol oxidation (with parallel or consecutive reactions) generates intermediates such as carbon monoxide (CO). CO strongly adsorbs at the catalyst surface, poisoning its active sites, and decreasing the FC efficiency [10].

Conventionally, alcohol-fuelled FCs use acid proton-exchange membranes and platinum-based catalysts [11]. The catalysts (Pt or other highly active materials) develop a critical role in the cost and durability of the FC system [3]. The Pt-based anodes and cathodes represent 35–42% of the total FCs cost. Therefore, since the partial oxidation pathway (without the release of 12 e^{-}) dominates on pure Pt catalysts, the greatest challenge in developing catalysts for ethanol oxidation is to facilitate C–C bond cleavage and thereby total oxidation at low potentials [9]. For this purpose, some strategies have been widely applied, such as (i) the incorporation of more oxyphilic materials, (ii) the modification of the catalyst morphology, and (iii) the change/modification on the support material.

DEFCs still suffer from the limited activity and stability of Pt NPs, even for the best catalysts. These problems are derived from the loss of Pt electrochemical surface area (ESA) over time, caused by the corrosion of carbon support and Pt dissolution/aggregation. Pt NPs possess high surface energies that induce severe Ostwald ripening and/or grain growth during the operation of the FC [12]. One-dimensional (1D) structures (such as NWs or nanotubes) may exhibit greater stability than NPs, whilst retaining high mass activities owing to (i) their high surface-area-to-volume ratio, (ii) the presence of large areas of smooth crystal planes and (iii) lower number of surface defect sites [13].

In this paper, we studied the electrocatalytic activity of carbon-supported Pt NWs towards ethanol and CO-monolayer oxidation in acidic media. The Pt/C NWs were synthesised without the use of any surfactant, template, or stabilising agent, and were compared with a commercial Pt/C reference catalyst. The comparison enabled the study of the effects caused by the morphology modification previously suggested by the study of single-crystal surfaces [14] to develop further highly active electrocatalysts, which may be successfully applied as anodes for DEFCs. Notably, we demonstrate that the NW morphology has a positive effect on the catalytic activity of the catalyst showing almost 2-fold higher mass activity in comparison with the commercial NPs Pt catalyst.

2. Experimental

2.1 Nanowires synthesis

Pt NWs were synthesised by the chemical reduction of the metallic precursor by formic acid [12,14] without the utilisation of surfactants, template, or stabilising agents. For the preparation of 100 mg of catalyst, 5.31 mL of hexachloroplatinic acid solution (0.03861 mol L^{-1}) (Sigma-Aldrich®, 37.5% of Pt) was dissolved in 4 mL of ultrapure water and left in an ultrasonic bath (Ultronique QR500) for ~30 min. The hexachloroplatinic acid solution was diluted to a total volume of 80 mL with ultrapure water, and 60 mg carbon black Vulcan XC-72R powder was added to the solution (to give a loading of 40 wt% Pt in the resulting catalyst) and stirred for 15 min. Then, 7.24 mL of pure formic acid (CH_2O_2, Sigma-Aldrich®, 98–100%) was slowly added, and the suspension was stirred for more 15 min. The resulting solution was stored for 72 h to allow the NWs growth, during which the solution changed from black to colourless (indicating the successful reduction of metallic precursors), and the resulting catalyst powder dropped down to the bottom of the reaction flask. The resulting suspension was vacuum-filtered, washed several times with ultrapure water and dried in an oven for 30 min at 60 °C, and finally stored for further electrochemical and physical characterisations. This catalyst is referred to as Pt/C NWs in the text below.

A commercial nanoparticle Pt/C (Pt on carbon black, from Johnson Matthey™) was used as a reference catalyst and is referred to as Pt/C NPs in the text below.

2.2 Physical characterisation

The XRD patterns were obtained using a Brucker D8 Advance diffractometer operating with Cu Kα radiation (λ = 0.15406 nm) machine. The patterns were generated at 50 kV and 100 mA with a scanning speed of 2° min^{-1} and sweep range between 20° and 90°. The diffractograms were compared with the JCPDS (Joint Committee of Powder Diffraction Standard) crystallographic cards. The morphology of the catalysts and their sizes were observed by transmission electron microscopy (TEM) using an FEI Tecnai 12 at an 80-kV accelerating voltage.

2.3 Electrode preparation and electrochemical measurements

The electrochemical measurements were performed at room temperature in 0.5 mol L^{-1} H_2SO_4 aqueous solution saturated with high purity N_2 (White Martins, 99.9 %) to eliminate dissolved O_2. All experiments were carried out in a conventional one compartment Pyrex® glass three-electrode electrochemical cell, using an Autolab Model PGSTAT 302N potentiostat/galvanostat. A Pt spiral wire was used as the counter electrode, a reversible hydrogen electrode (RHE) prepared at the same electrolyte solution immersed in a Luggin capillary was used as the reference electrode, and a glassy carbon disk (GC, 3 mm in diameter) was used as working electrode. The supporting electrolyte was used to produce hydrogen in the reference electrode, by applying a constant negative potential of –6.0 V. All aqueous solutions used at this work were prepared with ultrapure water (Gehaka model MS 2000 system, 18.2 MΩ·cm).

Before the measurements, the GC electrode was polished with a 0.3 µm α-alumina slurry, then, washed with 2-propanol and sequentially with ultrapure water in an ultrasonic bath, to remove the surface residues and renew the electrode surface, before each experiment. Electrocatalyst inks were prepared by adding 2.9 mg of the catalyst to a solution composed of 1000 µL of 2-propanol and 30 µL of 5 wt. % Nafion® (~5% lower aliphatic alcohols, Sigma Aldrich®). The resulting ink was sequentially submitted to an ultrasonic bath for 20 min for the dispersion and homogenization of the powder catalysts in the solution. 5 µL of the catalyst ink was deposited dropwise to the GC electrode surface and dried at room temperature.

For all electrochemical measurements, the catalyst ink modified GC electrodes were first submitted to 500 voltammetric cycles between 0.05 and 0.80 V at 500 mV s^{-1} to obtain reproducible voltammograms in 0.5 mol L^{-1} H_2SO_4 aqueous solution.

Cyclic voltammograms were recorded over 0.05 V to 1.30 V (2 cycles) performed at 20 mV s^{-1}. The electrochemically active surface area (ECA) was determined by integration of the monolayer hydrogen desorption peaks of the voltammograms (0.0–0.3 V) using a charge density of 0.21 mC cm^{-2} [15] and all electrochemical results presented below are normalised by the ECA.

The irreversible/adsorbed Bi process was used to quantify the number of {111} surface sites present in the catalysts, according to the method established by Feliu and co-workers [16, 17]. Thus, a cyclic voltammogram was obtained in the potential range of 0.05–0.75 V at 50 mV s^{-1} in 0.5 mol L^{-1} H_2SO_4 aqueous solution. The glassy carbon electrode was removed from the solution and washed with ultra-pure water. Then, the CV electrode was immersed in a solution containing Bi_2O_3 (10^{-4} mol L^{-1} of Bi) in $HClO_4$ (0.6 mol L^{-1}) for 1 min (enough time for the total covering of the sites (111) of the Pt). Bi_2O_3 was previously calcined at 500 °C for 45 min. Finally, the electrode was immersed into a 0.5 mol L^{-1} H_2SO_4 aqueous solution, and a new voltammogram was collected.

For the study of the EOR, ethanol was added (C_2H_6O, Sigma Aldrich, 99.5 %) until a 0.5 mol L^{-1} concentration and additional cyclic voltammograms were recorded. Derivative voltammetry was used to obtain more precise information regarding the EOR mechanism. The derivative voltammograms were constructed from the derivative of the first cycle of ethanol oxidation voltammogram, between 0.05 and 1.2 V *versus* RHE.

CO stripping experiments were carried out in 0.5 mol L^{-1} H_2SO_4 by first bubbling CO gas into the electrochemical cell for 5 min applying 0.05 V *versus* RHE, followed by purging with high purity N_2 for 25 min to remove the CO remaining in the solution. Sequentially, the CO stripping voltammogram was obtained (1 cycle) between 0.05 V and 1.30 V *versus* RHE at 20 mV s^{-1}.

In situ infrared spectroscopic measurements

In situ Fourier Transform Infrared (FTIR) measurements were carried out on a Bruker VERTEX 70v FTIR spectrometer equipped with an MCT detector cooled with liquid nitrogen. The reflectance spectra were collected with an R/R_0 ratio, in which R represents the spectra at a given potential, and R_0 is the collected spectra where no reaction of interest happens, in our case, 50 mV. Besides, the spectra were calculated from the average of 128 interferograms, with the spectral resolution set at 4 cm^{-1}. The *in situ* spectroelectrochemical system was equipped with a CaF_2 window, and the spectra were scanned between 3000 and 1000 cm^{-1} wavelength range.

The catalytic suspension was supported on a gold substrate previously polished with alumina (0.05 μm), to obtain a surface with high reflectivity. The catalyst was characterised in an H_2SO_4 0.5 mol L^{-1} solution and transferred to the spectroelectrochemical cell to investigate the EOR by *in situ* FTIR (in real-time). Then, ethanol (0.5 mol L^{-1}) was added, and the spectra were collected as a function of the applied potential. The scan rate and the number of interferograms were chosen to allow the spectra to be collected at intervals of about 0.05 V between 0.05–1.0 V of potential *versus* RHE.

3. Results and discussion

3.1. Physical characterisation

Fig. 1 shows the TEM micrographs of the commercial Pt/C NPs (Fig.1A) and the synthesised Pt/C NWs catalyst (Fig.1B). Pt NWs were successfully synthesised by the formic acid as the reducing agent methodology, as demonstrated by the presence of well-defined multi-armed star-like Pt NWs in the images. In Fig. 1B, Pt NWs are composed of several short arms approximately 20 nm in length and 4 nm diameter. The good dispersion of the Pt NWs over the carbon support may indicate a favourable interaction between the metallic atoms and the exposed crystal planes of the carbon [18]. The selected-area diffraction (SEAD) pattern (Fig. 1B inset) reveals a series of bright concentric rings, which are attributed to face-centred cubic (fcc) structure of crystal Pt, which is similar to that of bulk Pt [19,20]. These bright rings are assigned to {111} (inner ring), {200}, {220} and {311} (outer ring) planes, confirming that this method produces highly crystalline NWs [18-20].

The powder XRD patterns for the commercial Pt/C NPs and the synthesised Pt/C NWs catalysts are shown in Fig. 2. The XRD patterns were compared with the JCPDS (Joint Committee of Powder Diffraction) crystallographic cards. Similar peak positions are observed for both catalysts. The diffraction peak at $2\theta = 26.54°$ is ascribed to the graphite carbon (PDF card no. 001-0646). For both catalysts, the peaks at $2\theta = 39.91°$, 46.44°, 67.75°, 81.60°, and 86.21° are assigned to *fcc* phase of Pt reflections planes (111), (200), (220), (311) and (222), respectively, in accordance with PDF card no. 004-0802, in agreement with TEM images shown in Fig.1.

The Pt(220) diffraction peak (inset) shifted slightly to higher 2θ values, attributed to the NWs anisotropic structure[21]. As previously reported by Sun et al. [22], the reduction reaction used to form the NW at room temperature proceeds slowly, favouring the anisotropic growth according to the lowest energy principle. For *fcc* structures, the order of surface energies is (111) < (100) < (110), and therefore, the relative growth rate along the closed-packed <111> direction is increased. However, the exact growth mechanism is not fully known [21].

In order to evaluate the metallic loading of the catalysts, EDX measurements were recorded (Fig. S1). The EDX analysis confirmed that the metallic loading of the as-prepared Pt/C NWs catalyst (40.7±0.53 wt%) and for Pt/C NPs (19.5±0.10 wt%) is close to the nominal values, respectively, 40 and 20 wt%, as expected.

3.2. Electrochemical characterisation

Fig. 3 shows the cyclic voltammograms (second scan), recorded in 0.5 mol L^{-1} H_2SO_4 between 0.05 V and 1.30 V *versus* RHE at 20 mV s^{-1}, for the synthesised NWs catalyst and commercial NP Pt/C. Both catalysts show typical profiles of carbon-supported Pt-based catalysts in acidic media [23]. The voltammograms display pairs of well-defined peaks in the hydrogen adsorption/desorption region (0.05 to 0.30 V *versus* RHE), with differences in the desorption peaks attributed to preferential exposure of multiple crystallographic planes [24] for the NWs catalyst.

Comparison to the published cyclic voltammograms of single-crystal Pt electrodes [24], suggests that for the Pt/C NWs catalyst, the main peaks at ~0.11 V and ~0.27 V (0.21 V for the commercial Pt/C catalyst) *versus* RHE show can be attributed to H adsorbed on (110) steps and (100) step sites on (111) terraces, respectively. For the Pt/C NWs, the peak corresponding to (100) step sites on (111) terraces, which arise from (111) x (111) junction, is more pronounced. The commercial catalyst showed a broader second peak, which is attributed to contributions from short (110) terraces or kinks, indicative of the NP (cubooctahedral or icosahedral) shape. The presence of a peak at ~0.55 V for the synthesised Pt/C NWs catalyst may also be an indication of the presence of (111) terraces contribution [24], although this peak overlaps with region often attributed to the quinone/hydroquinone couple on the carbon support [25].

Fig. 4 shows the voltammetric profiles recorded in 0.5 mol L^{-1} H_2SO_4 between 0.05 V and 0.75 V *versus* RHE at 50 mV s^{-1} before and after Bi adsorption for Pt/C NPs (Fig 4a) and Pt/C NWs (Fig. 4b) catalysts. In order to estimate the fraction of (111) ordered domains present on the catalysts surface, bismuth irreversible adsorption was carried out (red dashed lines at Fig. 4a and 4b). The charge measured under the peak at 0.62 V was used to determine the charge associated with (111) terrace sites present on the surface of the catalyst [16, 17]. The Pt/C NPs and Pt/C MWs yield charge density values of 16.3 and 50.2 µC cm^{-2}, respectively, which corresponds, using the calibration equation (Equation 1) [17], to a charge associated with (111) terrace sites of 25.5 and 78.4 µC cm^{-2}.

$$q_{Bi} = 0.64 q_{\{111\}}^{t-1} \quad (1)$$

These values indicate that the surface of Pt/C NPs and Pt/C MWs have a ratio, respectively, of 11.6 and 35.6 % of (111) ordered domains. These results indicate that NWs morphology enhanced the existence of (111) terrace sites.

The monolayer CO stripping peaks have previously been investigated at single crystal Pt surfaces, and their positions and shapes related to different symmetries and size domains over the catalyst surfaces reported [26]. For example, Lai et al. [27] employed a combination of electrochemical and theoretical techniques to study the CO and methanol electro-oxidation on stepped single-crystal Pt and Rh electrodes. They studied the mechanism and kinetics of CO electro-oxidation on Pt electrode on a number Pt[*n*(111) x (111)] vicinal surfaces. For an *fcc* metal, these surfaces are composed of terraces of (111) orientation, which are (n – 1) atoms wide, separated by monoatomic steps of (110) orientation. In the CO oxidation study, a pronounced catalysing effect of steps was observed. Higher step density lowers the overpotential of CO oxidation with peak potentials difference for Pt(553), and Pt(111) equals 0.17 V between them. This effect was attributed to the preferential formation of O-containing species at the steps sites compared to the terrace sites.

Fig. 5 shows the CO-monolayer stripping voltammograms. The hydrogen desorption region (0.0–0.20 V *versus* RHE) is entirely suppressed on both catalysts, confirming the saturation of the surfaces of the catalyst with adsorbed CO (CO_{ads}) [28]. The voltammogram for the Pt/C NPs is in excellent agreement with those presented in the literature, for carbon-supported Pt NPs recorded at 20 mV s^{-1} [29]. This catalyst shows CO oxidation only above 0.60 V with a single peak (peak III) centred at ~0.82 V. In contrast, the voltammogram for the Pt/C NWs has three peaks, peak I at 0.45 V, peak II at 0.73 V, and peak III overlapping with that of the Pt/C NPs.

The pre-peak (peak I) is commonly known as pre-ignition or pre-oxidation wave [30] and has been the subject of many studies, with several explanations proposed, including (i) the shift of bridge-bonded CO (CO_b, weakly adsorbed) to linear-bonded CO (CO_L, strongly adsorbed), (ii) preferential oxidation of CO_b, (iii) oxidation of a weakly adsorbed or kinetically unstable CO state, (iv) preferential oxidation at or near defect sites and (v) the oxidation been driven by a rearrangement of CO-induced by the potential [31].

However, based on Farias and co-worker's publication [31], the occurrence of the CO peroxidation peak is controlled by four interconnected and simultaneous conditions, such as CO adsorption at potentials lower than about 0.2 V; on surfaces saturated with CO_{ads}; in the presence of both, traces of CO solution and surface steps. If any of these four conditions is not satisfied, the CO preoxidation pathway does not appear. For example, in Farias et al.'s paper, they compare the CO oxidation in the presence and absence of small amounts of dissolved CO in the electrolyte. In these experiments, the potential was fixed at 0.1 V, and CO was bubbled into the solution for 5 min to cover the electrode surface fully. After that, Ar was bubbled into the solution for 5, 10, and 60 min. Finally, when the solution was purged for 60 min, the CO peroxidation signal became utterly absent. Thus, based on our experimental setup, were CO adsorption was hold at 0.05 V for 5 min, and N_2 was bubbled for 25 min; we believed that these four conditions are satisfied.

The sharp peak II in Fig. 5 for the Pt/C NWs catalyst on 0.73 V is comparable with the "butterfly" peak, which is observed in CO oxidation in perchloric solution [32]. This peak appears in 0.1 mol L^{-1} $HClO_4$ solution and corresponds to the reversible adsorption of OH (OH_{ads}). In this sense, this peak, in 0.5 mol L^{-1} H_2SO_4 solution, may be attributed to a filling-in process by OH_{ads} on the Pt defects in the closed-packed adlayer [33]. However, the formation of a full OH_{ads} adlayer on the H_2SO_4 solution is inhibited due to the strong adsorption [34].

For instance, the effect of Pt agglomeration on CO stripping must be considered. According to Mailard et al. [35], platinum agglomeration can cause peak II, observed for the Pt/C NWs catalyst. Also, according to Urchaga et al. [36], the multiple peaks on CO stripping could be related to the presence of different crystal facets at the Pt surface. It was indicated that larger particles have a higher number of exposed faces Pt(111) on their surface than in small Pt nanoparticles. It is also known that the Pt(111) face is more thermodynamically stable and, therefore, it would be the most preferably exposed surface in the case where the particles agglomerate [37]. Thus, it is likely that peak II for the Pt/C NWs catalyst is due to the oxidation of weakly adsorbed CO on Pt(111) faces, present in large quantities in both agglomerated Pt particles and nanowires, compared to isolated Pt nanoparticles. This fact becomes evident from the CO stripping profile (Fig. 5) for the catalyst with nanoparticle morphology, Pt/C NPs, in which peak II is absent. Thus, the Peak III present in both catalysts, centred at 0.82 V and 0.83 V for Pt/C NPs and Pt/C NWs, respectively, can be attributed to the oxidation of CO adsorbed in isolated Pt nanoparticles.

Fig. 6 shows the cyclic voltammograms for EOR obtained at room temperature and 20 mV s^{-1} scan rate. Both catalysts presented the characteristic profile of the ethanol oxidation in acidic media on carbon-supported Pt. The hydrogen adsorption region was fully inhibited, indicating strong adsorption of ethanol molecules at the catalysts surface active sites at the initial potential of 0.05 V. Significant voltammetric changes were observed with the morphology change from NPs to NWs. The Pt/C NPs catalyst showed smaller EOR currents at all potentials, with an onset potential of ~0.73 V, chosen as the potential at which the current density was 5 mA cm^{-2}. In contrast, the synthesised Pt NWs catalyst displayed approximately 5-fold greater EOR current densities, with a much lower ethanol oxidation onset potential (~0.57 V). The negatively shifted onset potential is comparable with that reported for state-of-art bimetallic catalysts [38].

Fig. 7 shows the first derivatives of the anodic sweep for Pt/C NPs and Pt/C catalysts, using the method described by Murthy and Manthiram [39]. Some insights regarding the ethanol oxidation mechanism can be obtained by using derivative voltammetry; however, up to now, a detailed ethanol oxidation mechanism remains unclear, since many parallel and consecutive reactions can happen, resulting in more than forty possible volatile and adsorbed species [40,41]. Currently, a dual-pathway mechanism on Pt catalysts is broadly accepted for either acid or alkaline environments: [14,42]

C1 pathway: $CH_3 - CH_2OH + 3H_2O \rightarrow 2CO_2 + 12H^+ + 12e^-$ (2)

$$CH_3 - CH_2OH + 5H_2O \rightarrow 2HCO_3^- + 14H^+ + 12e^- \quad (3)$$

$$CH_3 - CH_2OH + 5H_2O \rightarrow 2CO_3^{2-} + 16H^+ + 12e^- \quad (4)$$

C2 pathway: $CH_3 - CH_2OH + H_2O \rightarrow CH_3 - COOH + 4H^+ + 4e^-$ (5)

$$CH_3 - CH_2OH \rightarrow CH_3 - CHO + 2H^+ + 2e^- \quad (6)$$

The C1 pathway leads to the complete ethanol oxidation to CO_2 through the CO_{ads} intermediate delivering 12 e^-. Hence, the C2 pathway represents the partial oxidation of ethanol to acetate or acetic acid (both delivering 4 e^-) and to acetaldehyde (delivering 2 e^-) without the C–C bond cleavage [43]. At low potential (< 0.4 V), the ethanol oxidation starts with the adsorption of ethanol at the Pt surface (equation 7). Furthermore, adsorbed ethanol can suffer oxidation to acetaldehyde or CO (derived from the dissociative adsorption, equations 8 to 12). Besides, reaction 5 occurs preferentially at potentials higher than 0.8 V, in which water molecule is activated, forming O-containing species. Reaction 6 illustrates acetaldehyde production. This reaction happens preferentially at potentials below 0.6 V, where the dissociative adsorption of water occurs (reaction not shown) [44].

$$CH_3CH_2OH_{bulk} \rightarrow CH_3CH_2OH_{ads} \quad (7)$$

$$CH_3CH_2OH_{bulk} \rightarrow CH_3CHOH_{ads} + H^+ + e^- \quad (8)$$

$$CH_3CH_2OH_{ads} \rightarrow CH_3CHO_{ads} + H^+ + e^- \quad (9)$$

$$CH_3CHO_{ads} \rightarrow CH_3CHO_{bulk} \quad (10)$$

$$CH_3CH_2OH_{ads} \rightarrow CH_x + CO_{ads} \qquad (11)$$

$$CO_{ads} + OH_{ads} \rightarrow CO_2 + H^+ + e^- \qquad (12)$$

The derivative curves in Fig. 7 display two positive peaks, which are more defined for the Pt/C NWs catalyst. The electrocatalytic behaviour is similar for both catalysts between 0.2 and 0.4 V, which is the region where dissociative adsorption and the subsequent hydrogen removal occurs, resulting in CO_{ads}. Then, the derivative current starts to grow (for both catalysts) and stops at around 0.82 V (Peak II). In this region, the oxidation of CO_{ads} (equation 12) to CO_2 can be the rate-determining step (*rds*) for the catalysts. Peak I in Figure 7 (~ 0.73 V) is related to EOR through the C1 pathway (total oxidation); consequently, the higher this peak, the greater the amount of ethanol being oxidised. If this pathway did not happen, this peak would not exist (dashed arrow); hence, the C2 pathway would be dominating.

The Pt/C NWs catalyst shows the highest peak I, which can be associated with the ethanol's adsorption on the exposed crystal planes or defects of the NWs. The further increase of the potential around 0.83 V leads to more coverage of Pt sites with OH, blocking the ethanol adsorption and consequently decreasing the EOR, resulting in the third peak at both catalysts.

The Pt/C NPs catalyst showed the lowest ethanol oxidation, which can be explained by the high affinity of Pt for intermediary carbonaceous species, evidenced by the higher amount of LCAs. The derivative current reaches its minimum value at ~0.96 V for both catalysts, since, at this point, OH species are strongly adsorbed at the catalyst's sites, blocking the adsorption of ethanol from the bulk solution. In Fig.7, the ethanol oxidation onset potential for Pt/C NPs and Pt/C NWs catalysts are 0.67 and 0.60 V, respectively, which are very close to the values obtained at cyclic voltammetry tests (Fig. 6).

Chronoamperometric curves in Fig. S2 shows that the Pt/C NWs catalyst displays the highest anodic current density (0.0062 mA cm^{-2}) that is more than 5-fold higher the current density presented by the commercial Pt/C NPs (0.0012 mA cm^{-2}) at the end of the experiment. Those data agree with the results in Fig. 6, indicating a better EOR and less coverage of the surface by intermediate by-products for the synthesised catalyst, which derives from the unique NW morphology.

The polarisation curves (Fig. S3) confirms the trend in both Figs. 5 and 7, indicating enhanced ethanol oxidation activity for the synthesised Pt/C NWs. The change in catalysts the morphology (NPs to NWs) shifts the oxidation onset potential to more negative values (Table 1).

Table 1. CO and ethanol oxidation onset potential and Tafel slopes for all catalysts synthesised in this study

Catalyst	**CO oxidation E_{onset} [V]**	**Ethanol oxidation E_{onset} [V]^a**	**Current density at 900 s [mA cm^{-2}]^b**	**Tafel slopes [mV dec^{-1}]**	**Mass activity (A mg^{-1}_{Pt}) @ [0.8 V *versus* RHE^a]**
Pt/C NPs	0.77	0.41	0.0012	180.32	0.007
Pt/C NWs	0.68	0.36	0.0062	134.15	0.013

^{a} Values obtained by Tafel plots.

^{b} Values obtained by chronoamperometric experiment.

The Tafel slopes were 180.32 and 134.15 mV dec^{-1} for Pt/C NPs and Pt/C NWs catalyst, respectively, indicating that different rate-determining steps (*rds*) can be happening for both catalysts [20,45]. Tafel slopes around 120 mV dec^{-1} have been obtained on single-crystal carbon-supported Pt catalysts. Generally, the Tafel slope allows the observation of whether the *rds* is the transfer of the first or second electron and if a chemical reaction is involved [46]. Thus, for the synthesised Pt/C NWs catalyst, the obtained slope value (close to 120.0 mV dec^{-1}) is in agreement with a mechanism that involves Temkin-type adsorption for both OH_{ads} and ethoxy at low potentials [47]. For the commercial Pt/C NPs catalyst, the value of 180.32 mV dec^{-1} indicates that the *rds* is controlled by the ethanol dehydrogenation or acetic acid formation or a combination of both [48]. Further, different Tafel slopes can also be obtained depending on the distribution of by-products [49].

FTIR experiments were carried out to understand the formation of products and intermediates and the effect of the catalyst morphology on the EOR. The main functional groups related to ethanol oxidation products are listed in Table 2.

Table 2: Assignment of the bands observed in the spectra obtained by FTIR

Wavenumber (cm^{-1})	**Functional group or chemical species**	**Deformations**	**References**
2980, 2903	CH_3, CH_2	C–H, stretch	[50]
2621	COOH	O–H, stretch	[50]
2343	CO_2	O=C=O, asymmetrical stretch	[51]
2050	CO_L	–C–O, stretch	[52]
1720	COOH ou CHO	–C=O, carbonyl stretch	[51]
1650	H_2O	H–O–H, angular deformation	[53]
1400	Acetate	–O–C–O, stretch	[54]
1367	Acetaldehyde	–CH_3, symmetrical stretch	[55, 56]
1280	Acetic acid	–C=O, stretch	[51]
1200	HSO_4^{2-}	S–O, symmetrical and asymmetrical stretch	[57]
1113	Acetaldehyde	C–H, vibration	[56]
1045	Ethanol	C–O, axial deformation	[58]

Fig. 8 shows the *in situ* FTIR reflectance spectra acquired over a potential range of 0.05–1.0 V *versus* RHE, in which the spectra were obtained every 0.05 V in H_2SO_4 0.5 mol L^{-1} + ethanol 0.5 mol L^{-1} solution on the Pt/C NPs and Pt/C NWs catalysts. Pointing down bands (negative bands), indicate the species formation between the thin layer of the working electrode and the CaF_2 window, on the other hand, pointing upwards bands (positive bands), represent the consumption/decrease of another species. The presence of CO_2, acetaldehyde, and acetic acid was observed for both catalysts, indicating that both pathways are present (C1 and C2 pathway).

The upward band located at 1650 cm^{-1} is assigned to the bending mode H–O–H of water [49]. This band is more intense for the Pt/C NWs catalyst (Fig. 8a) than for the Pt/C NPs catalyst. A more intense positive water band for Pt/C NWs can implicate that more water is consumed or that more water is leaving the thin layer region. Water is oxygen donor species, necessary for alcohols oxidation to CO_2, also competes with the organic molecules for adsorption sites [55]. In this sense, as the Pt/C NWs catalyst showed the highest intensities in the CO_2 bands, more considerable amounts of water are needed to complete the reaction, which may justify the higher positive water bands for the catalyst with nanowire morphology. Parallel to this, as the by-products are formed, water is expelled from the thin layer to permit the diffusion of the new products generated. Since the Pt/C NWs catalyst generated the largest bands of CO, CO_2, and CH_3COOH, a higher amount of water is expelled from the thin layer.

Three upwards bands detected at 1045 cm^{-1}, 2903 cm^{-1}, and 2980 cm^{-1} are ascribed to axial deformation of C–O, and ethanol asymmetric CH_2, and CH_3 vibrations, respectively [59] indicates the consumption of ethanol from the thin layer.

The negative band at 2343 cm^{-1} is attributed to asymmetrical stretch O=C=O of CO_2. The first band of CO_2 appears from 0.75 V for Pt/C NPs and 50 mV earlier for Pt/C NWs, which are in good agreement with CO monolayer oxidation (Fig. 4), and the signal of the band increases with increasing potential. It is worth to note that the band at 2343 cm^{-1} for Pt/C NWs catalyst (Fig. 7b) is much more intense than Pt/C NPs catalyst, indicating that a more significant amount of CO_2 may be produced. As previously mentioned, the existence of extended terraces or defects on the NW catalyst could result in enhanced mobility of OH_{ads} and CO_{ads}, facilitating the CO oxidation from the catalyst surface [60].

The band at 2050 cm^{-1} is attributed to the C–O stretch of linearly adsorbed CO (CO_L) [52]. CO_L band was initially detected at 0.45 V for Pt/C NPs and 0.4 V for Pt/C NWs. The appearance of these bands indicates that the breaking of the C–C bond of the ethanol molecule occurs between 0.05 and 0.45 V, resulting in the formation and accumulation of adsorbed CO. The intensity of this band reaches the maximum between 0.6 and 0.65 V for both catalysts. Subsequent decay of CO_L band intensity may be a consequence of both increased oxidation of adsorbed CO and decreased CO_L formation. However, for Pt/C NWs the CO_L band intensity is still present up to 1.0 V, which differs from data obtained during CO stripping measurements (Fig. 5), where all CO molecules have been oxidised to CO_2 at 1.0 V in both catalysts. These discrepancies will be explained further below.

The band located at 1720 cm^{-1} is associated with the stretching vibration of the carbonyl group C=O [51] present in acetic acid and acetaldehyde. For the Pt/C NPs catalyst, the first band was observed at 0.75 V, and for Pt/C NWs catalyst, the band was identified at 0.65 V. From these potentials, the band continuously increases until reaching 1.0 V and the formation of intermediates without the C–C bond breaking seems to be predominant [61].

Acetic acid formation becomes evident from the bands located at 2621 and 1280 cm^{-1}, attributed to the –OH stretching deformation and –C=O stretching groups, respectively. These bands appear only at high potentials, 0.65 V for Pt/C NWs, and higher than 0.75 V for Pt/C NPs. Another band located at 1400 cm^{-1} at high potential values was identified as the stretching of adsorbed acetate (–O–C–O), indicating that acetate can be an intermediate of ethanol oxidation reaction [53].

The bands at 1367 and 1113 cm^{-1} are associated with symmetric deformation (–CH_3) and vibration (C–H), respectively, of acetaldehyde [55]. The 1113 cm^{-1} band was initially observed at 0.65 V for Pt/C NPs and 0.70 V for Pt/C NWs, and its intensity continuously increased to 1.0 V for both catalysts. Acetaldehyde formation occurs first, then the formation of acetic acid, which confirms that acetaldehyde is an intermediate for the production of acetic acid, as previously demonstrated by Iwasita et al. [62] and Weaver et al. [63].

For all materials, it is possible to observe the stretching bands of the HSO_4^- ion at 1200 cm^{-1}, due to the H_2SO_4 used as the electrolyte [53]. The HSO_4^- band is due to its accumulation in the thin layer in order to compensate for the positive increase of electrode potential [55].

For a more detailed analysis of infrared spectra, the absorption area of the bands of CO (2050 cm^{-1}), CO_2 (2343 cm^{-1}), and acetic acid (1280 cm^{-1}) was integrated. After integration, these areas were normalised by the electroactive area of each electrode obtained during the CO oxidation experiments (Fig. 5). The dependences of the integrated band intensities of Pt/C NPs and Pt/C NWs catalysts on the potential are shown in Fig. 8. It should be noted that these graphs indicate at which potential the ethanol oxidation reaction products are generated, they do not allow the quantification of these products. However, the results suggest that CO, CO_2, and CH_3COOH production for Pt/C NWs is much higher than Pt/C NPs, which can explain the increased oxidation current density obtained during the cyclic voltammograms (Fig. 6).

Fig. 9a shows the behaviour of the intensity of integrated CO absorption bands. The CO band intensities for the catalysts increases as the potential increases up to 0.6 and 0.65 V for Pt/C NPs and Pt/C NWs, respectively. At potentials higher than 0.6 V for Pt/C NPs and 0.65 V for Pt/C NWs, the CO_L band starts to decrease. For the commercial Pt/C NPs, the CO_L band is no longer visible in the spectra at potentials higher than 0.85 V. These outcomes may indicate the total elimination of adsorbed CO or a slow rate of C–C bond breaking. However, this band is still present for the Pt/C NWs until 1.0 V. Del Colle *et al*. [64] suggested that the presence of the CO_L band at high potentials means that the CO is being produced at a rate higher than the oxidation rate and, consequently, some CO remains on the surface. Nevertheless, it seems more plausible to assume that some CO is present from both, the reference (0.05 V) and the sampling potentials (0.1–1.0 V), thus generating a bipolar band with some contribution of the CO_L bands at higher potentials [64], thereby justifying the presence of CO_L bands at potentials as high as 1.0 V.

Note in Fig. 9b that the onset potential for CO_2 production was 0.7 V for both catalysts. However, the production of CO_2 was higher on Pt/C NWs catalyst than on commercial Pt/C NP catalyst in all potentials studied (Fig. 9b). This fact may be due to the existence of extended terraces or defects on NWs morphology [60]. Moreover, a surface contraction may occur for the Pt nanowires. According to Nørskov and Hammer's theory, [65, 66] a surface contraction strain can cause a down-shift of the d-band centre of Pt, which will decrease the absorption strength of reactants. Wang et al. [67] reported a down shift of the Pt 4f d-band for Pt NWs compared to Pt NPs supported on carbon. Thus, this structure-dependent electronic change of the Pt/C NWs may improve the CO surface diffusion rate due to the weaker binding of CO, leading to an enhanced oxidation rate.

Another comment about the effect of the morphology of the nanowire is related to O/OH adsorption. At high potentials, there is a competition on the catalyst surface between

O/OH and ethanol adsorption. Similar to the CO poisoning effect, the strong interaction of O/OH and the surface of the catalyst could block the active sites and decrease the ethanol oxidation rate. Therefore, a surface with a weaker OH binding strength can provide more sites for ethanol oxidation [55]. Observing the displacement, for higher potentials, of the Pt–O reduction peak for the nanowire morphology catalyst (Fig. 3), the lower binding energy between Pt and the oxygenated species can be suggested for the nanowire morphology catalyst, justifying the higher catalytic activity compared to the catalyst with nanoparticle morphology.

Acetic acid has been formed at potentials higher than 0.6 V in both Pt/C NPs and Pt/C NWs catalysts. For potentials higher than 0.75 V, the acetic acid bands for Pt/C NWs were higher compared to commercial Pt/C NPs. Previous results [68] indicated that the (111) plane is very active in the formation of acetic acid, and an increase in the <111> direction for Pt/C NWs could explain the higher production of acetic acid.

In summary, from FTIR data, it was possible to observe that the C1 pathway, with the C–C bond break to CO formation, is dominant in both surfaces, Pt/C NWs and Pt/C NPs, at low potentials, lower than 0.6 V. However, at higher potentials, the production of acetic acid and acetaldehyde took place and the C2 pathway which represents the partial oxidation of ethanol, maintaining the C–C bond intact, is the main path.

3. Conclusions

This paper describes the synthesis of carbon-supported Pt NWs using a simple, low cost, template-free, and surfactant-less chemical reduction of metallic precursors method by formic acid. TEM images confirmed the formation of NWs of approximately 20 nm in length and 4 nm in diameter, confirming the success of the applied methodology for the synthesis.

The synthesised NWs presented improved catalytic activity compared with the commercial Pt/C Johnson Matthey catalyst, showing higher oxidation current density, as well as, lower onset potentials for ethanol and CO-monolayer oxidation, attributed to the presence of (110) step sites on (111) terraces. The oxidation current density was more than 5-fold higher than the commercial NPs catalyst for EOR measured at 0.90 V *versus* RHE. FTIR results revealed the presence of CO, CO_2, acetic acid, and acetaldehyde for all catalysts, demonstrating that both routes C1 and C2 are active for these catalysts. However, the nanowires produced more significant quantities of CO_2.

The results confirm the feasibility of the synthesis method and the importance of the nanowire morphology in the removal of intermediate species from the catalyst surface, producing efficient catalysts to be applied as anodes for DEFCs.

Acknowledgements

The authors would like to thank CNPq (grants: 305438/2018-2, 407274/2013-8, 400443/2013-9, 474261/2013-1, 304419/2015-0, and 310282/2013-6), to the *Coordenação de Aperfeiçoamento de Pessoal de Nível Superior* - CAPES (grant: 88881.121097/2016-01), to FAPITEC/SE, Brazil, and The Royal Society and the Newton Fund (NMG\R1\180416 - Newton Mobility Grants 2018 Round 1) for financial support and scholarships.

4. References

[1] A. Kirubakaran, S. Jain and R. K. Nema, A review on fuel cell technologies and power electronic interface, Renew. Sustain. Energy Rev. 13 (2009) 2430.

[2] E. Antolini, Catalysts for direct ethanol fuel cells, J. Power Sources 170 (2007) 1.

[3] K. Vignarooban, J. Lin, A. Arvay, S. Kolli, I. Kruusenberg, K. Tammeveski, L. Munukutla and A. M. Kannan, Nano-electrocatalyst materials for low temperature fuel

cells: A review, Cuihua Xuebao/Chinese J. Catal. 36 (2015) 458.

[4] M. M. de Souza, R. S. Gomes and A. L. de Bortoli, A model for direct ethanol fuel cells considering variations in the concentration of the species Int. J. Hydrogen Energy 43 (2018) 1.

[5] A. Sayadi and P. G. Pickup, Evaluation of ethanol oxidation catalysts by rotating disc voltammetry, Electrochim. Acta 215 (2016) 84.

[6] M. A. F. F. Akhairi and S. K. Kamarudin, Catalysts in direct ethanol fuel cell (DEFC): An overview, Int. J. Hydrogen Energy 41 (2016) 4214.

[7] C. Lamy, E. M. Belgsir and J. M. Léger, Electrocatalytic oxidation of aliphatic alcohols: Application to the direct alcohol fuel cell (DAFC), J. Appl. Electrochem. 31 (2001) 799.

[8] F. A. Zakil, S. K. Kamarudin and S. Basri, Modified Nafion membranes for direct alcohol fuel cells: An overview, Renew. Sustain. Energy Rev. 65 (2016) 841.

[9] M. Li, W. P. Zhou, N. S. Marinkovic, K. Sasaki and R. R. Adzic, The role of rhodium and tin oxide in the platinum-based electrocatalysts for ethanol oxidation to CO_2, Electrochim. Acta 104 (2013) 454.

[10] L. A. Soares, C. Morais, T. W. Napporn, K. B. Kokoh and P. Olivi, Beneficial effects of rhodium and tin oxide on carbon supported platinum catalysts for ethanol electrooxidation, J. Power Sources, 315 (2016) 47.

[11] M. Z. F. Kamarudin, S. K. Kamarudin, M. S. Masdar and W. R. W. Daud, Review: Direct ethanol fuel cells, Int. J. Hydrogen Energy 38 (2013) 9438.

[12] S. Sun, G. Zhang, D. Geng, Y. Chen, R. Li, M. Cai and X. Sun, A highly durable platinum nanocatalyst for proton exchange membrane fuel cells: Multiarmed starlike nanowire single crystal, Angew. Chemie - Int. Ed. 50 (2011) 422.

[13] Y.-H. Wen, R. Huang, Z.-Z. Zhu and Q. Wang, Mechanical properties of platinum nanowires: An atomistic investigation on single-crystalline and twinned structures,

Comput. Mater. Sci. 55 (2012) 205.

[14] S. C. S. Lai, T. M. Koper, The Influence of Surface Structure on Selectivity in the Ethanol Electro-oxidation Reaction on Platinum, J. Phys. Chem. Lett. 1 (2010) 1122.

[15] C. Zhang, L. Xu, Y. Yan and J. Chen, Controlled Synthesis of Pt Nanowires with Ordered Large Mesopores for Methanol Oxidation Reaction, Sci. Rep. 6 (2016) 1.

[16] J. Clavilier, J. M. Feliu, A. Aldaz, An irreversible structure sensitive adsorption step in bismuth underpotential deposition at platinum electrodes, J. Electroanal. Chem. 243 (1988) 419.

[17] J. Solla–Gullón, P. Rodríguez, E. Herrero, A. Aldaz, J. M. Feliu, Surface characterization of platinum electrodes, Phys. Chem. Chem. Phys. 10 (2008) 1359.

[18] E. S. Valério Neto, M. A. Gomes, G. R. Salazar-Banda and K. I. B. Eguiluz, Pt and Pt–Rh nanowires supported on carbon and SnO_2:Sb nanoparticles for ethanol electrochemical oxidation in acidic media, Int. J. Hydrogen Energy 43 (2018) 178.

[19] S. Sun, D. Yang, G. Zhang, E. Sacher and J. P. Dodelet, Synthesis and characterization of platinum nanowire–carbon nanotube heterostructures, Chem. Mater. 19 (2007) 6376.

[20] S. Sun, F. Jaouen and J.-P. Dodelet, Controlled growth of Pt Nanowires on carbon nanospheres and their enhanced performance as electrocatalysts in PEM fuel cells, Adv. Mater. 20 (2008) 3900.

[21] S. Wang, S. P. Jiang, X. Wang and J. Guo, Enhanced electrochemical activity of Pt nanowire network electrocatalysts for methanol oxidation reaction of fuel cells, Electrochim. Acta 56 (2011) 1563.

[22] S. Sun, G. Zhang, D. Geng, Y. Chen, M. N. Banis, R. Li, M. Cai and X. Sun, Direct growth of single-crystal Pt nanowires on Sn@CNT nanocable: 3D electrodes for highly active electrocatalysts, Chem. - A Eur. J. 16 (2010) 829.

[23] D. Ruan, F. Gao and Z. Gu, Enhanced electrochemical properties of surface roughed Pt nanowire electrocatalyst for methanol oxidation, Electrochim. Acta 147 (2014) 225.

[24] S. Sun, D. Yang, D. Villers, G. Zhang, E. Sacher and J. P. Dodelet, Template- and Surfactant-free room temperature synthesis of self-assembled 3D Pt nanoflowers from single-crystal nanowires, Adv. Mater. 20 (2008) 571.

[25] M. R. Tarasevich, G. V. Zhutaeva, V. A. Bogdanovskaya, M. V. Radina, M. R. Ehrenburg, A. E. Chalykh, Oxygen kinetics and mechanism at electrocatalysts on the base of palladium–iron system, Electrochim. Acta 52 (2007) 5108.

[26] Q. S. Chen, J. Solla-Gullón, S. G. Sun and J. M. Feliu, The potential of zero total charge of Pt nanoparticles and polycrystalline electrodes with different surface structure. The role of anion adsorption in fundamental electrocatalysis, Electrochim. Acta 55 (2010) 7982.

[27] S. C. S. Lai, N. P. Lebedeva, T. H. M. Housmans and M. T. M. Koper, Mechanisms of carbon monoxide and methanol oxidation at single-crystal electrodes, Top. Catal. 46 (2007) 320.

[28] I. J. McPherson, P. A. Ash, L. Jones, A. Varambhia, R. M. J. Jacobs and K. A. Vincent, Electrochemical CO oxidation at platinum on carbon studied through analysis of anomalous in situ IR spectra, J. Phys. Chem. C, 121 (2017) 17176.

[29] B. N. Grgur, N. M. Markovic, C. A. Lucas and P. N. Ross, Electrochemical oxidation of carbon monoxide: from platinum single crystals to low temperature fuel cells catalysts. Part I: Carbon monoxide oxidation onto low index platinum single crystals, J. Serbian Chem. Soc. 66 (2001) 785.

[30] M. J. S. Farias, G. A. Camara and J. M. Feliu, Understanding the CO preoxidation and the intrinsic catalytic activity of step sites in stepped Pt surfaces in acidic medium, J. Phys. Chem. C 119 (2015) 20272.

[31] Y. G. Yan, Y. Y. Yang, B. Peng, S. Malkhandi, A. Bund, U. Stimming and W. Bin Cai, Study of CO oxidation on polycrystalline Pt electrodes in acidic solution by ATR-SEIRAS, J. Phys. Chem. C 115 (2011) 16378.

[32] N. M. Marković, B. N. Grgur, C. A. Lucas and P. N. Ross, Electrooxidation of CO and H_2/CO mixtures on Pt(111) in acid solutions, J. Phys. Chem. B 103 (1999) 487–495.

[33] Q. S. Chen, A. Berna, V. Climent, S. G. Sun and J. M. Feliu, Specific reactivity of step sites towards CO adsorption and oxidation on platinum single crystals vicinal to Pt(111), Phys. Chem. Chem. Phys. 12 (2010) 11407.

[34] E. G. Ciapina, S. F. Santos and E. R. Gonzalez, Electrochemical CO stripping on nanosized Pt surfaces in acid media: A review on the issue of peak multiplicity, J. Electroanal. Chem. 815 (2018) 47.

[35] F. Maillard, S. Schreier, M. Hanzlik, E. R. Savinova, S. Weinkauf and U. Stimming, Influence of particle agglomeration on the catalytic activity of carbon-supported Pt nanoparticles in CO monolayer oxidation, Phys. Chem. Chem. Phys. 7 (2005) 385.

[36] P. Urchaga, C. Coutanceau and G. Jerkiewicz, Electro-oxidation of COchem on Pt nanosurfaces: Solution of the peak multiplicity puzzle, Langmuir 28 (2012) 3658.

[37] K. Kinoshita, Particle size effects for oxygen reduction on highly dispersed platinum in acid electrolytes, J. Electrochem. Soc. 137 (1990) 845.

[38] L. Jiang, A. Hsu, D. Chu and R. Chen, Ethanol electro-oxidation on Pt/C and PtSn/C catalysts in alkaline and acid solutions, Int. J. Hydrogen Energy 35 (2010) 365.

[39] A. Murthy and A. Manthiram, Application of derivative voltammetry in the analysis of methanol oxidation reaction, J. Phys. Chem. C 116 (2012) 3827.

[40] W.-P. Zhou, M. Li, C. Koenigsmann, C. Ma, S. S. Wong and R. R. Adzic, Morphology-dependent activity of Pt nanocatalysts for ethanol oxidation in acidic media: Nanowires versus nanoparticles, Electrochim. Acta 56 (2011) 9824.

[41] A. Kowal, M. Li, M. Shao, K. Sasaki, M. B. Vukmirovic, J. Zhang, N. S. Marinkovic, P. Liu, A. I. Frenkel and R. R. Adzic, Ternary Pt/Rh/SnO_2 electrocatalysts for oxidizing ethanol to CO_2, Nat. Mater. 8 (2009) 325.

[42] G. R. O. Almeida, E. M. Sussuchi, C. T. de Meneses, G. R. Salazar-Banda and K. I. B. Eguiluz, Influence of the metallic load of Pt/C and $Pt_{0.6}$-$Ru_{0.4}$/C nanowires on the electrochemical oxidation of methanol in acid medium, Int. J. Electrochem. Sci. 12 (2017) 7502.

[43] Y. Wang, S. Zou and W.-B. Cai, Recent advances on electro-oxidation of ethanol on Pt- and Pd-Based catalysts: From reaction mechanisms to catalytic Materials, Catalysts 5 (2015) 1507.

[44] L. C. Silva-Junior, G. Maia, R. R. Passos, E. A. de Souza, G. A. Camara and M. J. Giz, Analysis of the selectivity of PtRh/C and PtRhSn/C to the formation of CO_2 during ethanol electrooxidation, Electrochim. Acta 112 (2013) 612.

[45] Y. Bai, J. Wu, J. Xi, J. Wang, W. Zhu, L. Chen and X. Qiu, Electrochemical oxidation of ethanol on Pt–ZrO_2/C catalyst, Electrochem. commun. 7 (2005) 1087.

[46] H. B. Hassan, Electro-oxidation of ethanol and propanol at Pt and Ti modified nanoparticle substrates for Direct Alcohol Fuel Cells (DAFCs), Open Electrochem. J., 1 (2009) 19–27.

[47] A. Kapałka, G. Fóti and C. Comninellis, Determination of the Tafel slope for oxygen evolution on boron-doped diamond electrodes, Electrochem. commun. 10 (2008) 607.

[48] A. Bach Delpeuch, T. Asset, M. Chatenet and C. Cremers, Influence of the temperature for the ethanol oxidation reaction (EOR) on Pt/C, Pt-Rh/C and Pt-Rh-SnO_2/C, Fuel Cells 15 (2015) 352.

[49] A. Pushkarev, I. Pushkareva, N. Ivanova, S. du Preez, D. Bessarabov, R. Chumakov, V. Stankevich, V. Fateev, A. Evdokimov and S. Grigoriev, Pt/C and Pt/SnO_x/C Catalysts

for Ethanol Electrooxidation: Rotating Disk Electrode Stud, Catalysts 9 (2019) 271.

[50] G. Sócrates, Infrared and Raman Characteristic Group Frequencies: Tables and Charts. 3 ed. John Wiley & Sons, 2001.

[51] G. Sócrates, Infrared and Raman Characteristic Group Frequencies: Tables and Charts. 4 ed. John Wiley & Sons, 2004.

[52] C. V. S. Almeida, D. S. Ferreira, H. Huang, A. C. Gaiotti, G. A. Camara, A. E. Russell, K. I. B. Eguiluz and G. R. Salazar-Banda, Highly active Pt_3Rh/C nanoparticles towards ethanol electrooxidation. Influence of the catalyst structure, App. Catal. B: Environ. 254 (2019) 113.

[53] A. B. Delpeuch, F. Maillard, M. Chatenet, P. Soudant and C. Cremers, Ethanol oxidation reaction (EOR) investigation on Pt/C, Rh/C, and Pt-based bi- and tri-metallic electrocatalysts: A DEMS and in situ FTIR study, App. Catal. B: Environ. 181 (2016) 672.

[54] M. Li, W.-P. Zhou, N. S. Marinkovic, K. Sasaki and R. R. Adzic, The role of rhodium and tin oxide in the platinum-based electrocatalysts for ethanol oxidation to CO_2, Electrochim. Acta 104 (2013) 454.

[55] M. Li, A. Kowal, K. Sasaki, N., Marinkovic, D. Su, E. Korach, P. Liu and R. R. Adzic, Ethanol oxidation on the ternary Pt–Rh–SnO_2/C electrocatalysts with varied Pt:Rh:Sn ratios, Electrochim. Acta 55 (2010) 4331.

[56] J. G. Wu, Modern Fourier Transform Infrared Spectroscopy Techniques and their Applications. 1 ed. Scientific and Technical Document Publishing House, 1994.

[57] M. E. Paulino, L. M. Nunes, E. R. Gonzalez and G. Tremiliosi-Filho, In situ FTIR spectroscopic study of ethanol oxidation on Pt(111)/Rh/Sn surface. The anion effect, Electrochem. Commun. 52 (2015) 85.

[58] O. Guillén-Villafuerte, G. García, M. C. Arévalo, J. L. Rodríguez and E. Pastor, New insights on the electrochemical oxidation of ethanol on carbon-supported Pt electrode by a novel electrochemical mass spectrometry configuration, Electrochem. Commun. 63 (2016) 48.

[59] J. M. Perez, B. Beden, F. Hahn, A. Aldaz and C. Lamy, “In situ” infrared reflectance spectroscopic study of the early stages of ethanol adsorption at a platinum electrode in acid medium, J. Electroanal. Chem. 262 (1989) 251.

[60] W.-P. Zhou, M. Li, C. Koenigsmann, C. Ma, S. S. Wong and R. R. Adzic, Morphology-dependent activity of Pt nanocatalysts for ethanol oxidation in acidic media: Nanowires versus nanoparticles, Electrochim. Acta 56 (2011) 9824.

[61] E. Pastor and T. Iwasita, D/H exchange of ethanol at platinum electrode, Electrochim. Acta 39 (1994) 547.

[62] T. Iwasita, B. Rasch, E. Cattaneo and W. Vielstich, A SNIFTIRS study of ethanol oxidation on platinum, Electrochim. Acta 34 (1989) 1073.

[63] L.-W. H. Leung, S.-C. Chang, M. J. Weaver, Electrooxidation of ethanol and related species on well-defined Pt(111) surfaces, J. Electroanal. Chem. 266 (1989) 317.

[64] V. Del Colle, J. Souza-Garcia, G. Tremiliosi-Filho, E. Herrero and J. M. Feliu, Electrochemical and spectroscopic studies of ethanol oxidation on Pt stepped surfaces modified by tin adatoms, Phys. chem. chem. Phys. 13 (2011) 12163.

[65] B. Hammer, Y. Morikawa and J. K. Nørskov, CO chemisorption at metal surfaces and overlayers, Phys. Rev. Lett. 76 (1996) 2141.

[66] B. Hammer and J. K. Nørskov, Theoretical surface science and catalysis—calculations and concepts, Adv. Catal. 45 (2000) 71.

[67] S. Wang, S. P. Jiang, X. Wang and J. Guo, Enhanced electrochemical activity of Pt nanowire network electrocatalysts for methanol oxidation reaction of fuel cells,

Electrochim. Acta 56 (2011) 1563.

[68] F. Colmati, G. Tremiliosi-Filho, E. R. Gonzalez, A. Berná, E. Herrero and J. M. Feliu, Surface structure effects on the electrochemical oxidation of ethanol on platinum single crystal electrode, Faraday Discuss. 140 (2009) 379–397.

Figures

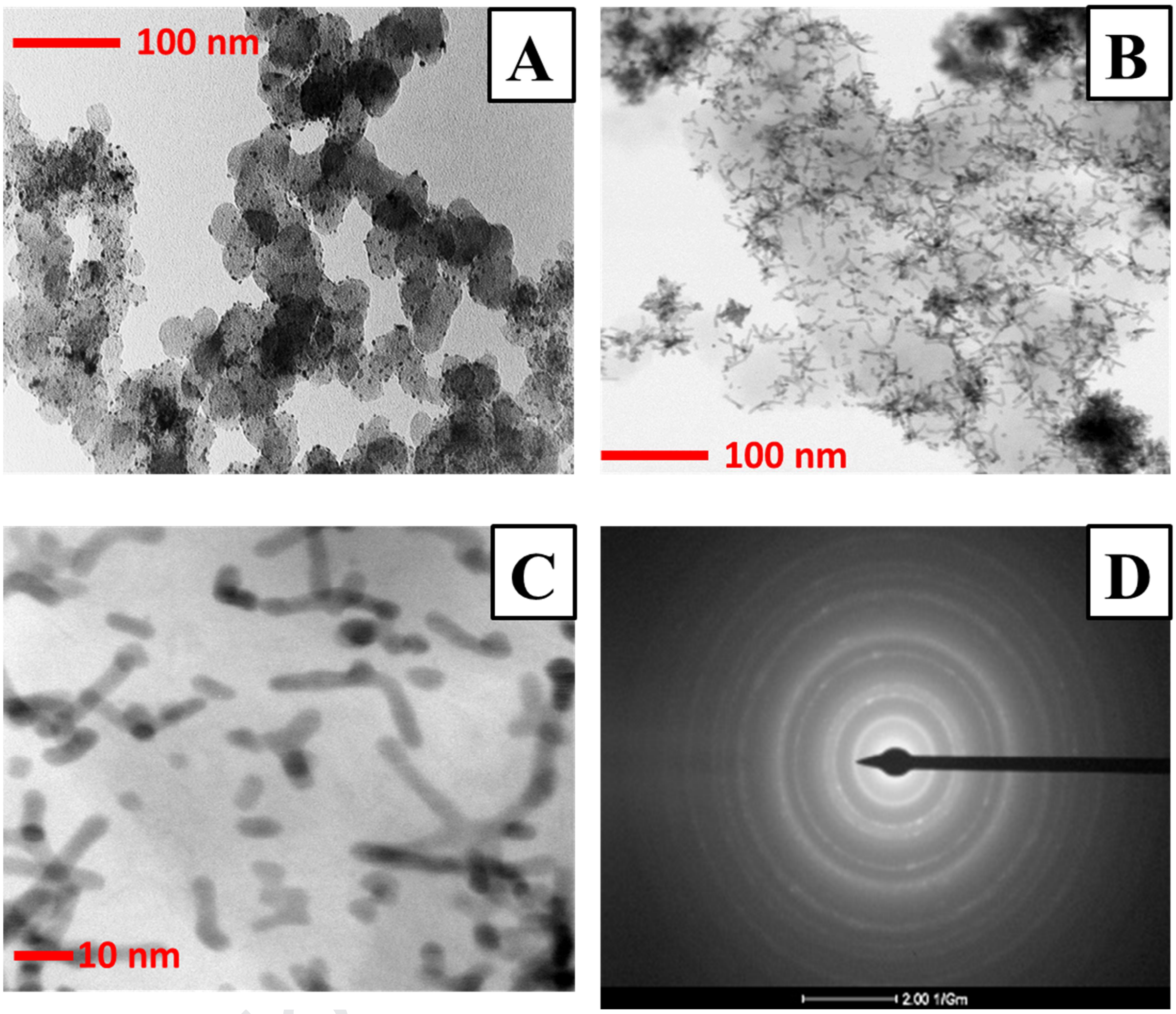

Figure 1. TEM micrographs obtained for (A) Pt/C NPs, and (B, C) Pt/C NWs catalysts in different magnifications, as well as (D) SAED pattern obtained for the Pt/C NWs catalyst.

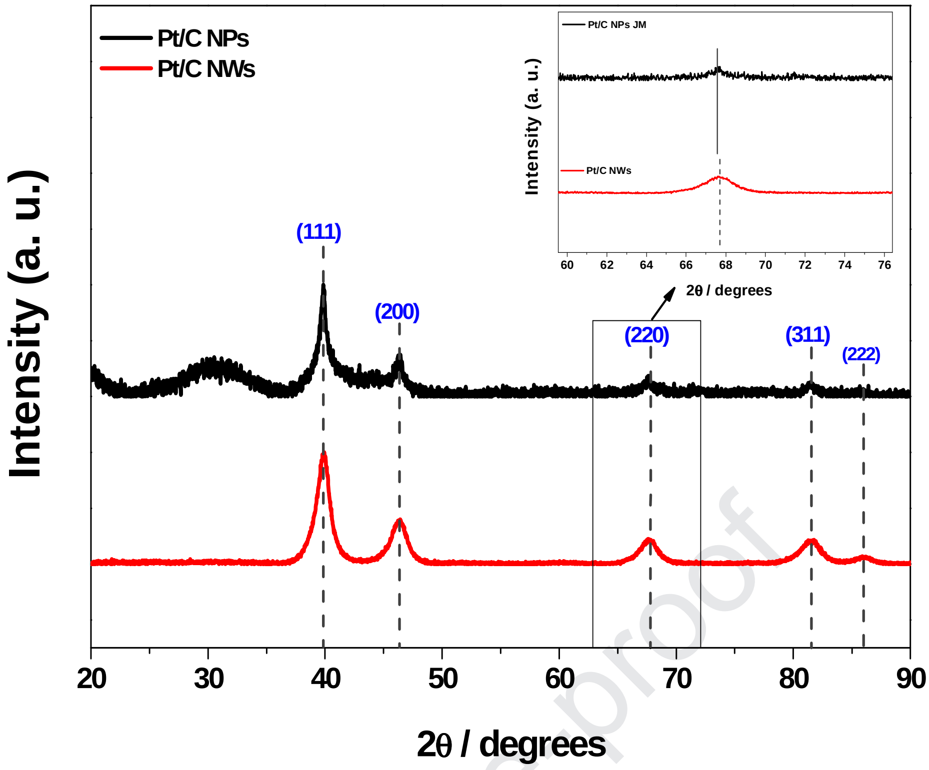

Figure 2. XRD patterns of the Pt/C NPs Johnson Matthey and Pt/C NWs catalysts. The inset is the enlarged Pt(220) diffraction peak for both catalysts.

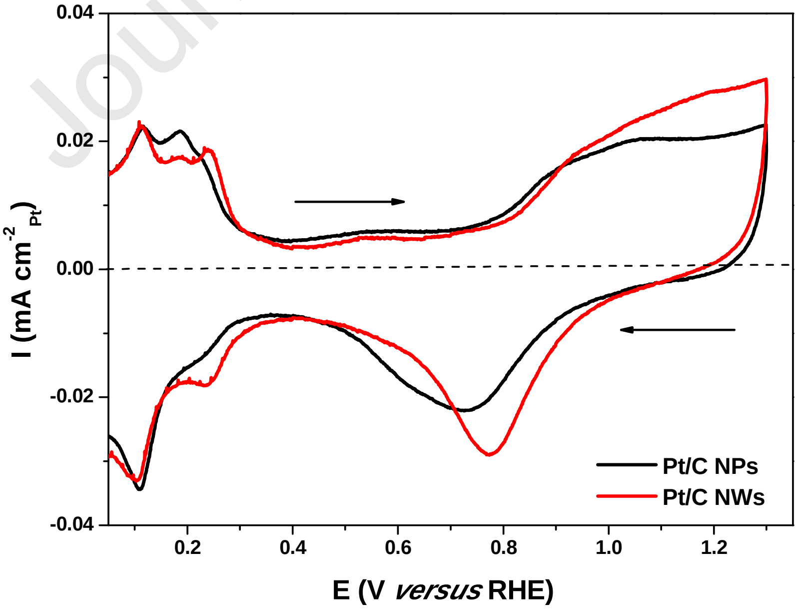

Figure 3: Cyclic voltammograms (second cycle) recorded in 0.5 mol L^{-1} H_2SO_4 for the Pt/C NPs Johnson Matthey and Pt/C NWs catalysts. υ = 20 mV s^{-1} and T = 25 °C.

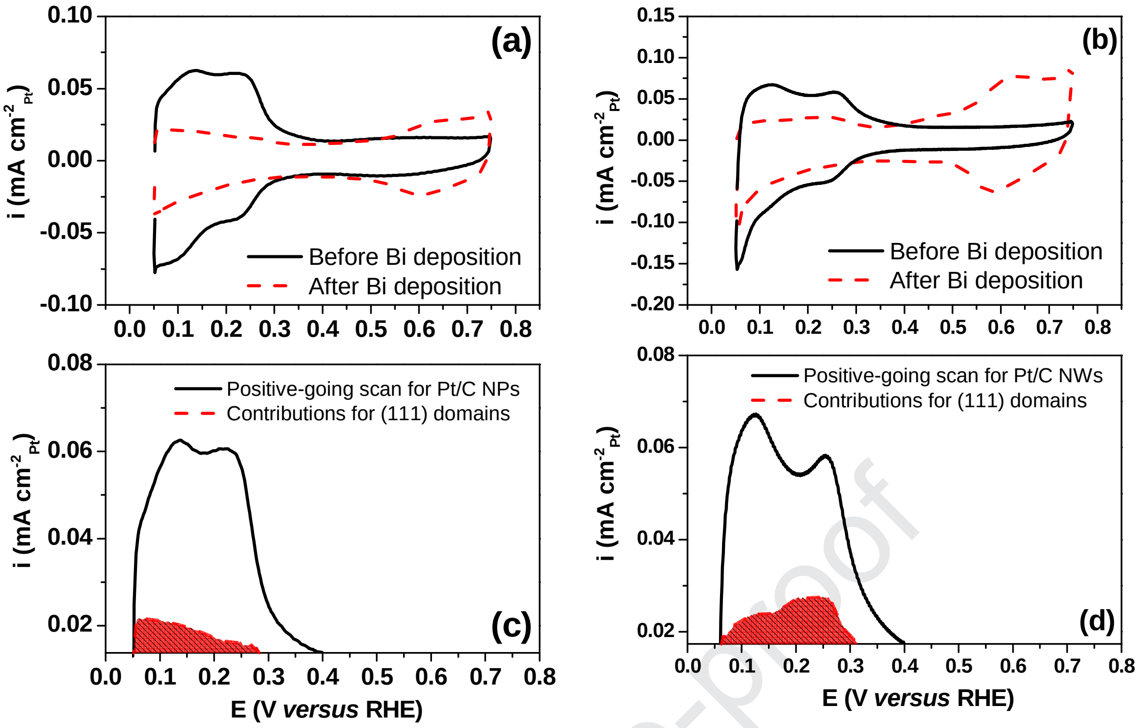

Figure 4: Voltammetric profiles before (black solid line) and after Bi deposition (red dashed line) for (a) Pt/C NPs and (b) Pt/C NWs. Positive going scan for (c) Pt/C NPs and (d) Pt/C NWs in the hydrogen adsorption/desorption region after double-layer subtraction in 0.5 mol L^{-1} H_2SO_4 and a scan rate of 50 mV s^{-1}. The shadowed area corresponds to the hydrogen contribution of the Pt atoms that were not covered by Bi.

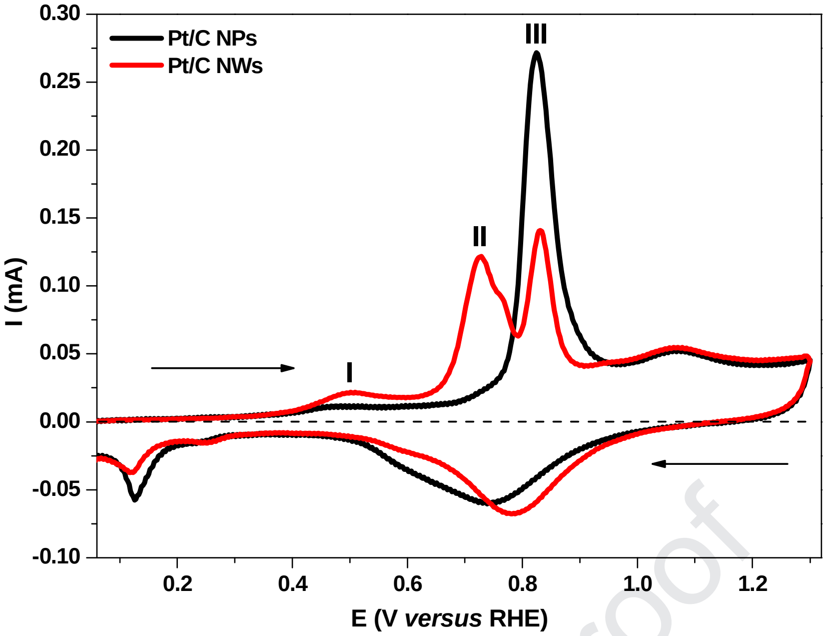

Figure 5. CO-monolayer stripping voltammetry (first scan) on Pt/C NPs Johnson Matthey and Pt/C NWs catalysts in 0.5 mol L^{-1} H_2SO_4 at 20 mV s^{-1}.

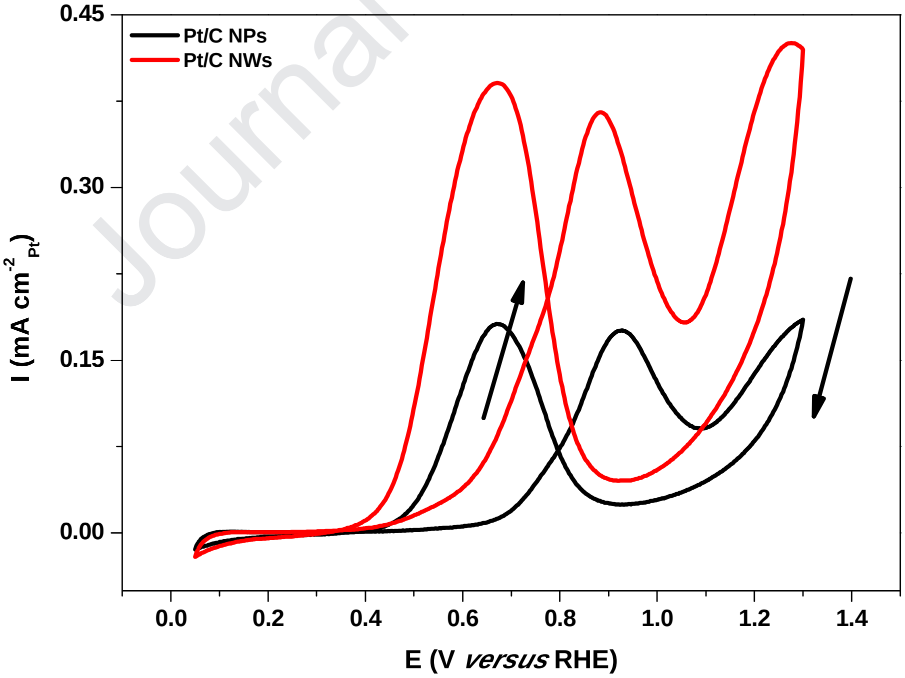

Figure 6. Cyclic voltammograms (second cycle) for the electrochemical oxidation of ethanol 0.5 mol L^{-1} dissolved in H_2SO_4 for Pt/C NPs Johnson Matthey and Pt/C NWs catalysts. υ = 20 mV s^{-1} and T = 25 °C.

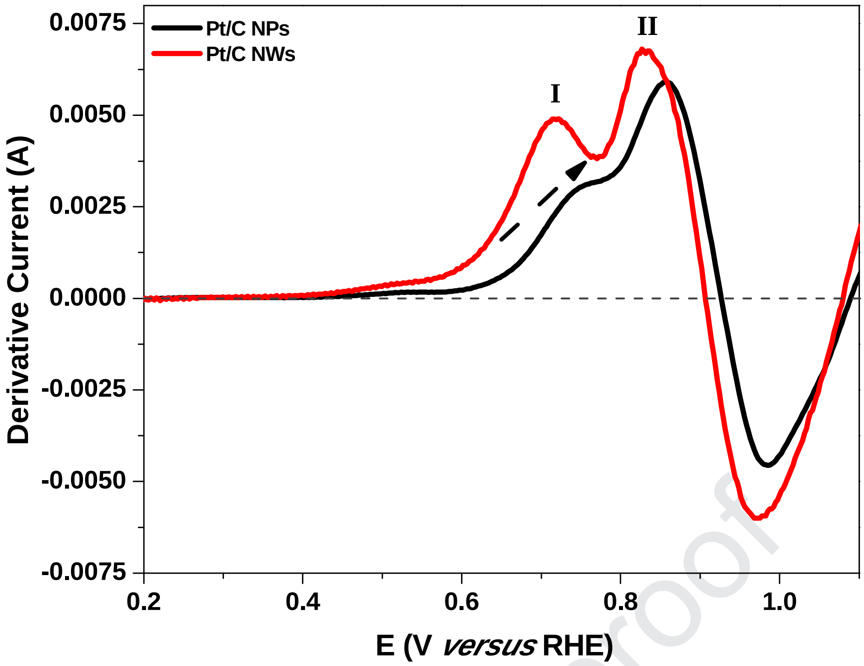

Figure 7. First derivative voltammograms of the anodic scans for ethanol oxidation on Pt/C NPs Johnson Matthey and Pt/C NWs catalysts obtained in 0.5 mol L^{-1} H_2SO_4 + 0.5 mol L^{-1} ethanol at 20 mV s^{-1}.

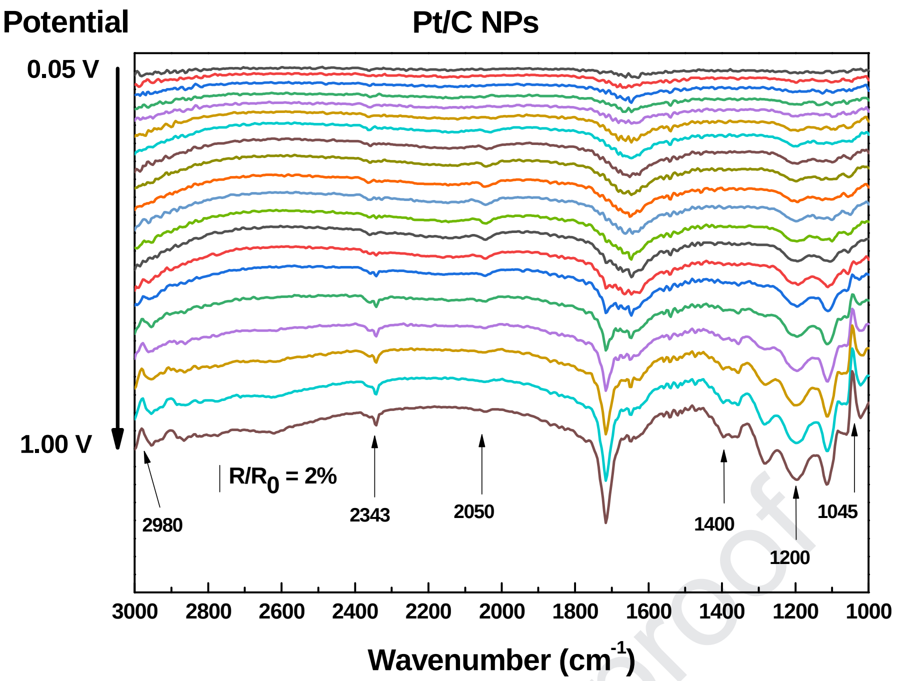

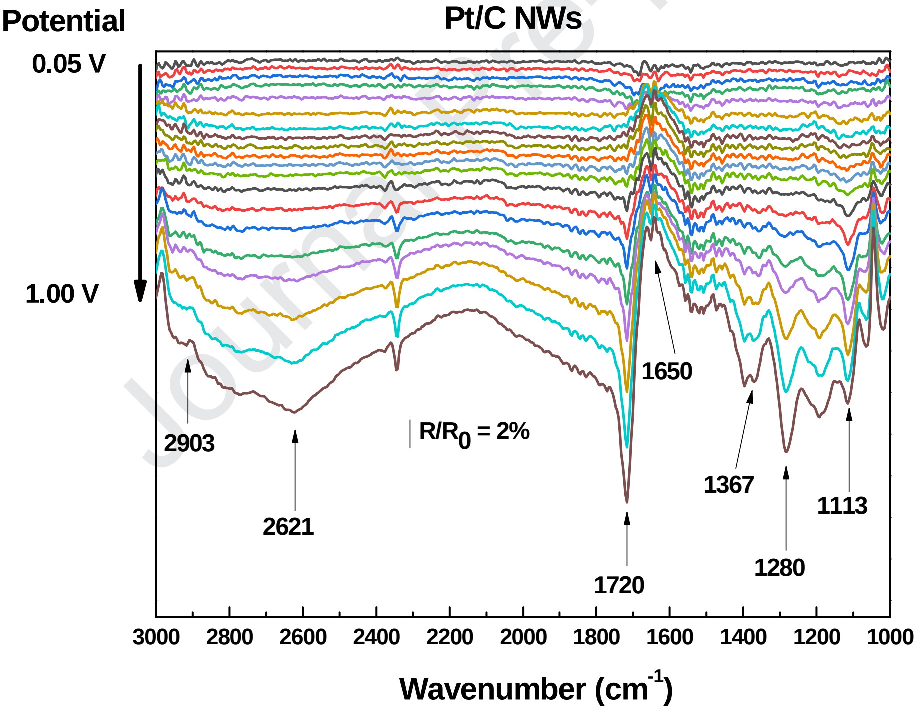

Figure 8: In situ FTIR spectra obtained during ethanol electrochemical oxidation on Pt/C NPs and Pt/C NWs catalysts, after 128 scans, H_2SO_4 0.5 mol L^{-1} + ethanol 0.5 mol L^{-1} solution. Reference spectra collected at 0.05 V during chronoamperometry steps and 4 cm^{-1} resolution. Potentials and compositions are indicated inside the figure.

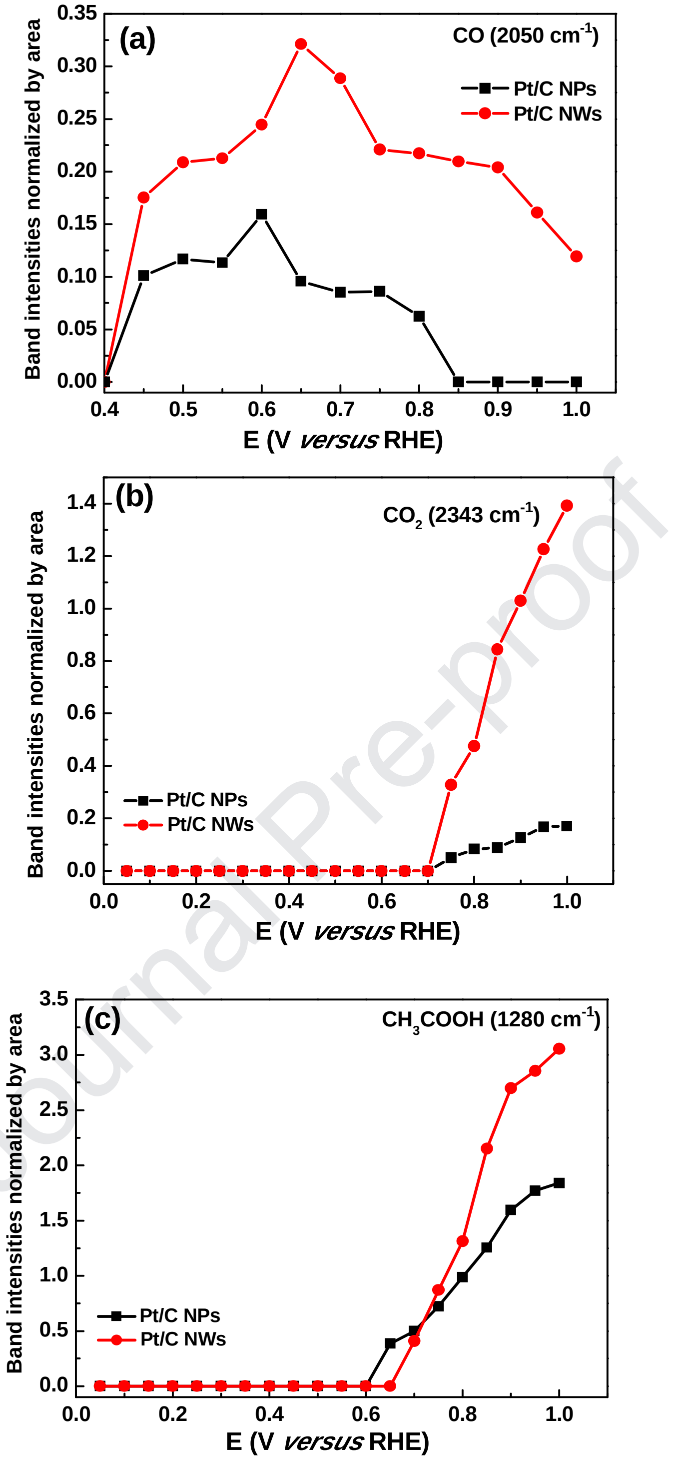

Figure 9: Intensity integration of (a) CO (2050 cm^{-1}), (b) CO$_2$ (2343 cm^{-1}), and (c) CH$_3$COOH (1280 cm^{-1}) bands obtained from the FTIR spectra of the Pt/C NPs and Pt/C NWs catalysts.

Highlights

- Pt/C nanowires were made without using surfactants, templates or stabilising agents
- The existence of extended terraces in NW catalysts improves ethanol electro-oxidation
- The current density for Pt/C NWs was 5-fold higher than the commercial NPs catalyst
- The nanowires morphology produces more significant quantities of CO_2 and acetic acid

Declaration of interests

☒ The authors declare that they have no known competing financial interests or personal relationships that could have appeared to influence the work reported in this paper.

☐The authors declare the following financial interests/personal relationships which may be considered as potential competing interests: